Accepted Manuscript

Calmodulin-induced conformational control and allostery underlying neuronal nitric oxide synthase activation

Quinlin M. Hanson, Jeffrey R. Carley, Tyler J. Gilbreath, Brian C. Smith, Eric S. Underbakke

PII: S0022-2836(18)30073-1
DOI: doi:10.1016/j.jmb.2018.02.003
Reference: YJMBI 65606

To appear in:

Received date: 15 December 2017
Revised date: 7 February 2018
Accepted date: 7 February 2018

Please cite this article as: Quinlin M. Hanson, Jeffrey R. Carley, Tyler J. Gilbreath, Brian C. Smith, Eric S. Underbakke , Calmodulin-induced conformational control and allostery underlying neuronal nitric oxide synthase activation. The address for the corresponding author was captured as affiliation for all authors. Please check if appropriate. Yjmbi(2018), doi:10.1016/j.jmb.2018.02.003

Calmodulin-induced conformational control and allostery underlying neuronal nitric oxide synthase activation.

Authors

Quinlin M. Hanson[1], Jeffrey R. Carley[1], Tyler J. Gilbreath[1], Brian C. Smith[2], and Eric S. Underbakke[a,1]

1 - Roy J. Carver Department of Biochemistry, Biophysics, and Molecular Biology, Iowa State University, Ames, IA 50011, USA;

2 - Department of Biochemistry, Medical College of Wisconsin, Milwaukee, WI 53226, USA

Correspondence to Eric S. Underbakke: 4212 Molecular Biology Building, 2437 Pammel Dr. Iowa State University, Ames, IA 50011, USA. 515-294-5793. esu@iastate.edu

Abstract

Nitric oxide synthase (NOS) is the primary generator of nitric oxide signals controlling diverse physiological processes such as neurotransmission and vasodilation. NOS activation is contingent on Ca^{2+}/calmodulin binding at a linker between its oxygenase and reductase domains to induce large conformational changes that orchestrate inter-domain electron transfer. However, the structural dynamics underlying activation of full-length NOS remain ambiguous. Employing hydrogen-deuterium exchange mass spectrometry, we reveal mechanisms underlying neuronal NOS (nNOS) activation by calmodulin and regulation by phosphorylation. We demonstrate that calmodulin-binding orders the junction between reductase and oxygenase domains, exposes the FMN subdomain, and elicits a more dynamic oxygenase active site. Furthermore, we demonstrate phosphorylation partially mimics calmodulin-activation to modulate nNOS activity via long-range allostery. Calmodulin-binding and phosphorylation ultimately promote a more dynamic holoenzyme while coordinating inter-domain communication and electron transfer.

Keywords

Hydrogen-deuterium exchange, mass spectrometry, allosteric communication, nitric oxide signaling

Abbreviations used:

nNOS, neuronal nitric oxide synthase; CaM, calmodulin; NO, nitric oxide; HDX-MS, hydrogen-deuterium exchange mass spectrometry; CT, *C*-terminal tail of nNOS; AI, auto-inhibitory element of nNOS; H4B, tetrahydrobiopterin.

Introduction

The diatomic gas nitric oxide (NO) serves dual physiological roles as both a signaling molecule and inflammation agent. Emitted at minute (nanomolar) concentrations, NO can function as a membrane-permeable paracrine signaling agent involved in cardiovascular and neurological functions [1-4]. Generated at high (micromolar) levels, NO acts as a potent cytotoxic weapon of the immune system. As a free radical, NO production is tightly regulated. Indeed, dysfunctional NO regulation is implicated in Alzheimer's and Parkinson's disease, excitotoxicity, auto-immune disorders, and cardiovascular disease [2-5]. Control over NO signaling is primarily exerted by regulating the localization and activation of the NO source, nitric oxide synthase (NOS).

The three mammalian NOS isozymes– endothelial NOS (eNOS), neuronal NOS (nNOS), and inducible NOS (iNOS)– share a general domain organization (Fig. 1a). The NOS isoforms are all homodimeric heme-containing oxidoreductases ranging from 260-320 kDa in molecular mass. The active site heme resides in an *N*-terminal oxygenase domain along with a catalytic tetrahydrobiopterin (H4B) cofactor. The *C*-terminal reductase domain is divided into an FAD/NADPH-binding subdomain and a mobile FMN subdomain. A regulatory calmodulin (CaM)-binding region connects the oxygenase and reductase domains. Activity of the constitutively expressed isoforms, eNOS and nNOS, is tightly regulated by the binding of Ca^{2+}/CaM. Conversely, conditional protein expression is the primary regulator of the constitutively active iNOS isoform, as Ca^{2+}/CaM binds iNOS irreversibly without elevation of cytosolic Ca^{2+} levels.

Interdomain conformational changes allow the NOS cofactors to deliver reducing equivalents from NADPH to the heme where L-arginine is converted to citrulline and NO. During catalysis, the FMN cofactor receives an electron in the reductase domain via a conformation known as the input state (Fig. 1b). The FMN subdomain then shuttles the reduced FMN to the heme cofactor by undergoing a large-scale conformational change to an output state, shifting the FMN subdomain to dock with the oxygenase domain to permit electron transfer to the heme [6-11]. CaM binding allows for productive transition from the input state to the output state, although the mechanism is not well understood [8, 12, 13]. CaM binding is thought to relieve regulatory constraints via unknown mechanisms to liberate the FMN subdomain from the

FAD/NADPH subdomains [7, 14]. Furthermore, CaM is thought to limit the conformational freedom of the FMN subdomain and direct it toward the output state while participating in the docking interaction with the oxygenase domain [7, 11, 15, 16].

In the absence of CaM, release from the input state is hypothesized to be constrained by several regulatory elements in the reductase domain: the autoinhibitory insert (AI) [17-19], the CD2A hairpin [20], and the *C*-terminal tail (CT) [21]. Importantly, these regulatory elements are unique to nNOS and eNOS, the two regulated NOS isoforms. Deletion of both AI and CT eliminates the CaM-dependence of electron flow through the reductase domain yet retains the CaM-sensitivity for overall NO production [22]. The CD2A hairpin is also thought to play a role in the reductase domain response to Ca^{2+}/CaM binding, although the mechanism remains unclear [20].

Recent single-particle EM studies revealed snapshots of accessible higher-order domain arrangements involved in the transit of the FMN subdomain between input and output states [7, 14]. However, the details of the CaM-induced conformational changes remain ambiguous. For example, the mechanism by which CaM releases the FMN subdomain from reductase regulatory elements to facilitate inter-domain shuttling is unclear. In addition, both the CT and AI regulatory elements contain phosphorylation sites that modulate eNOS and nNOS activity, adding another layer of complexity [21, 23, 24].

The lack of high resolution structures of full-length NOS holoenzymes obscures the structural basis for CaM-induced conformational changes and allostery. The three NOS isoenzymes have proven difficult to study by NMR and X-ray crystallography. Structures of NOS domain truncations have been reported but lack the context of a full-length enzyme [23, 25-28]. Crystal structures of the reductase domain informed current models of the input state [23]. However, observing the output state eludes the highest resolution structural techniques. Using hydrogen/deuterium exchange mass spectrometry (HDX-MS) and structural modeling, we previously developed a model of the output state for iNOS [11]. Nevertheless, the CaM-mediated dynamic conformational changes involved in transitioning between input and output states are poorly characterized. Here, we investigate mechanistic models of CaM-induced activation of NOS using HDX-MS.

HDX-MS is a useful technique for studying protein folding, protein–protein interactions, allostery, and conformational changes [29-34]. HDX-MS measures the rates of backbone amide proton exchange to report on local chemical environments. H/D exchange rates are influenced by secondary structure, hydrogen bonding, solvent exposure, and protein dynamics. As such, exchange rate perturbations are valuable indicators of local protein dynamics and allostery [35-38]. Indeed, HDX-MS was previously used to characterize the allostery and conformational changes associated with NO-induced activation of the NOS signaling partner, soluble guanylate cyclase [39]. We chose to determine the CaM-induced structural perturbations in the nNOS isozyme. nNOS in the brain regulates neurodevelopment and synaptic plasticity [3, 40-42]. NO produced by nNOS acts as a retrograde signaling molecule with putative collateral paracrine signaling effects. Strict regulation of nNOS activity is critical, as dysfunctional neuronal NO signaling is associated with excitotoxicity and neurodegenerative disorders [4, 5, 43]. Here, we present HDX-MS data describing the shift in conformational dynamics upon CaM-induced nNOS activation and modulation by phosphorylation.

Results

CaM Binding Perturbs Domain Interfaces and Regulatory Elements in the nNOS Reductase Domain.

CaM binding activates nNOS through mechanisms that are not fully understood. To determine the mechanism of nNOS activation by CaM, we employed HDX-MS. H/D exchange timecourses were collected for inactive nNOS and Ca^{2+}/CaM-activated nNOS. Deuterium incorporation of each uniquely identifiable peptic fragments was assessed using LC-MS. Increased rates of deuterium exchange result from disruptions in secondary structure and hydrogen bonding, increased dynamics or greater solvent accessibility. Conversely, decreased rates of deuterium exchange suggest local stabilization (e.g., formation of secondary structure and hydrogen bonding) or lower solvent accessibility. CaM-induced changes in nNOS exchange rates were mapped to the primary sequence and color coded (Fig. 2).

CaM-induced exchange rate perturbations were evident at several regions distributed throughout the holoenzyme. As expected, the region exhibiting the most

dramatic CaM-induced decreases in deuterium exchange rates (> 40%) was the CaM binding site (residues 731-744, Fig. 3a, Supplementary Fig. S1a). Exchange rate suppression extends to the short linker containing R752, a conserved residue believed to coordinate a hydrogen bond network between CaM and the FMN subdomain (Fig. 3b) [16, 44, 45]. Importantly, the observed peptide coverage enables a dissection of the contributions of the CaM-binding site and the adjacent linker. The peptide covering residues 749–758 excludes the direct CaM-binding region, allowing us to attribute strong exchange rate suppression to the linker itself (Supplementary Fig. S1b).

The stabilizing effect from the R752 linker also manifests at an FMN subdomain loop. This loop, comprising residues 777 to 781, includes residues engaged in a hydrogen-bonding network with R752 (R536 in human iNOS) in a reported structure of the isolated iNOS FMN subdomain bound to CaM (Supplementary Fig. S2) [16]. In contrast to the protection of regions adjacent to the CaM-binding site, the rest of the FMN subdomain manifests exchange rate increases (Fig. 3c). The deprotection upon CaM binding localizes, in part, to two loops surrounding the FMN cofactor (residues 806-815 and 886-892), which also form the input state interface with the FAD/NADPH lobe of the reductase domain (Supplementary Fig. S3). Surfaces thought to participate in the FMN—oxygenase domain interaction (including residues G810, N811, E819, and C823) also undergo significant deprotection [11, 44]. These findings are consistent with an overall increase in FMN subdomain exposure and/or mobility in CaM-activated nNOS.

Multiple regulatory elements reside in the reductase domain, including the CD2A hairpin, the AI, and the CT. The CD2A hairpin exhibits pronounced CaM-induced exchange rate increases primarily in a β-strand within the motif (Fig. 3c). This is likely due to a change in the local chemical environment due to the proximity of the bound CaM. Exchange rate perturbations were not evident in the CT or AI elements. However, deuterium incorporation had largely saturated in these elements before the first measured time point (15 s), obscuring possible effects at shorter time points. Nevertheless, pronounced increases in exchange rate are evident at FMN subdomain surfaces contacting these regulatory elements. In addition, a weak enhancement of exchange at NADPH/FMN subdomain residues 1382—1395 surrounds the AI, evidently

due to a CaM-induced conformational change influencing the contacts between the AI and FMN subdomain (Fig. 3d). Similarly, we observe perturbations upon CaM-binding on the surface of the FMN subdomain proximal to the CT (Fig. 3e).

CaM-Induced Conformational Effects in the nNOS Oxygenase Domain

HDX results mapped to the nNOS oxygenase domain reveal CaM-induced perturbations largely localized to the surfaces surrounding the heme electron transfer access point (Fig. 4a). A small hole around the putative FMN-oxygenase interface (forming the output state) allows access to the heme (Fig. 4b) [11, 16]. Deuterium exchange increases manifest at the "lip" of this heme access point (residues 416-424). Flanking this region, the outside edge of the oxygenase domain shows modest deuterium exchange rate increases. In addition, a short peptide encompassing W587 is also perturbed by CaM-binding (Fig. 4b, Supplementary Fig. S4). Tryptophan at this position is invariant across NOS isoforms that employ a flavodoxin reductase and plays a critical role in facilitating electron transfer from the FMN cofactor to the heme [11, 16, 46]. Together with the reductase domain results described above, perturbations at the heme access point and FMN subdomain appear to be the primary hallmarks of activated nNOS.

nNOS Phosphomimetic Variants Modulate NOS activity

Our results reveal that CaM binding induces striking exchange rate perturbations in regions surrounding known sites of phosphorylation in the AI and CT (Fig. 3d-e). Phosphorylation of AI residue S847 or CT residue S1412 modulates the activity of nNOS. In cells, S847 phosphorylation decreases the activity of nNOS [24, 47]. S1412 phosphorylation, on the other hand, stimulates nNOS signaling pathways [48-50]. Introducing substitutions of serine to aspartate often mimics the negative charge of a phosphoserine, serving as a phosphomimetic. Indeed, both S847D and S1412D mimic the modulation of nNOS behavior in cells [51]. Purified S847D recapitulates decreased nNOS activity observed in cells [52]. The effects of S1412D substitution largely manifest as increases in electron transfer flux through the reductase domain [53]. We aimed to determine the influence of phosphomimetics on nNOS structural dynamics and CaM-induced activation. To this end, we generated nNOS variants S847D and S1412D. Our

characterization of the steady state kinetics of NO production and electron transfer activity agree well with previous reports (Supplementary Fig. S5) [52, 53].

Phosphomimetic Variants of nNOS Demonstrate Synergistic Perturbations with CaM binding

Comparisons of the H/D exchange rates for CaM-activated S1412D and S847D relative to WT nNOS reveal additive conformational perturbations beyond the CaM-binding effects. Both phosphomimetic variants increase protection at the CaM-binding helix relative to WT nNOS, with no change in the R752 linker (Fig. 5). At the FMN subdomain both S847D and S1412D induce deuterium exchange increases, with the strongest perturbations near the FMN cofactor and putative output state interface. The effects of S847D and S1412D diverge in the oxygenase domains. CaM-stimulated S847D exhibits modest protection around the heme electron transfer access point (residues 416-424) and a moderate protective effect on the electron-conducting residue W587 relative to CaM-bound WT. Conversely, widespread deuterium exchange rate increases are observed in the oxygenase domain of S1412D nNOS. S1412D perturbs a broader surface than CaM-bound WT or S847D, suggesting the S1412D variant has a stronger effect on output state conformational dynamics. Taken together, these data suggest both nNOS phosphomimetic variants effect the input state population similarly but have differing ramifications on output state population.

Dissecting Contributions of Phosphomimetics and CaM in nNOS Activation

S847 and S1412 phosphorylation are thought to tune nNOS activity by disfavoring the input state conformation [51]. However, the conformational dynamics induced by S847 and S1412 phosphorylation was unclear. To test the allosteric consequences attributable to phosphorylation, we compared H/D exchange rates for the nNOS WT and phosphomimetic variants in the absence of CaM. Strikingly, both nNOS phosphomimetics manifested H/D exchange perturbations in both reductase and oxygenase domains (Supplementary Fig. S6). For both phosphomimetics the FMN subdomain was deprotected at surfaces adjacent to the sites of phosphorylation in the AI and CT. These perturbed FMN subdomain surfaces are also implicated in both the input and output state conformations. Surprisingly, both phosphomimetic variants also

showed subtle perturbations in the oxygenase domain. The heme access point exhibited increased perturbation due to S1412D and decreased perturbation in S847D. As these results parallel perturbations observed in the presence of CaM (Fig. 5), the dynamic changes observed appear to derive from the phosphomimetic variants.

Although the nNOS S847D and S1412D variants share some of the markers of activation independent of CaM (i.e., increased exchange at the FMN subdomain), neither phosphomimetic produces NO without CaM binding. While phosphorylation appears to potentiate the conformational dynamics of nNOS, CaM-binding induces a unique conformational effect required for productive NOS activity. To dissect the CaM-induced contributions to the activation of phosphomimetic nNOS variants, we compared CaM-free and CaM-bound S847D or S1412D nNOS (Supplementary Fig. S7). For both variants, CaM ordered the CaM-binding helix and reinstated the apparent rigidification of the R752-containing linker. Additionally, the CD2A hairpin showed increased deuterium exchange in both phosphomimetics. Furthermore, both variants exhibited enhanced deuterium exchange in the FMN subdomain at surfaces that participate in the output state. This was complemented by a further increase in deuterium exchange at the heme access point for the S1412D variant and further decrease for S847D. Taken together, the intrinsic conformational changes induced by nNOS S847D and S1412D variants share some features with CaM-activated WT nNOS. However, the increased dynamics associated with the phosphomimetics are insufficient to activate NO production. Our data suggest the following: i) FMN subdomain release is sensitive to multiple factors, ii) NO production depends on CaM to order the R752 linker and coordinate the FMN subdomain movement, and iii) conformational dynamics intrinsic to phosphomimetic variants can act synergistically (S1412D) or in opposition to (S847D) CaM-activation of nNOS.

Discussion

Illuminating the mechanisms by which CaM orchestrates the inter-domain shuttling of NOS is a prerequisite to understanding physiological control of NO signaling. HDX-MS of full-length nNOS and phosphomimetic variants, reported herein, allowed direct identification of key conformational changes in nNOS activation. Our data revealed that CaM-binding induces changes in dynamics and conformation

throughout the nNOS domains. Prominent structural perturbations localize to the heme electron transfer access point of the oxygenase domain (Fig. 4), the CaM binding linker, and key regulatory interfaces of the reductase domain (Fig. 3). Moreover, CaM-induced allosteric effects surround phosphorylation sites known to tune NOS activity. The phosphomimetic nNOS variants reveal how phosphorylation may induce significant conformational perturbations in nNOS (Fig. 6). Furthermore, comparison of CaM-bound and CaM-free phosphomimetics highlights the importance of CaM-specific conformational changes to productively communicate between reductase and oxygenase domains.

The most pronounced structural change for WT nNOS and the phosphomimetic variants due to CaM-binding appears in the CaM-binding linker. The strong protection elicited by CaM-binding is consistent with the high affinity of the interaction (K_d ~ 2-6 nM) [54, 55]. However, protein–protein interactions alone do not typically evoke such a strong protection; changes in backbone hydrogen-bonding, especially secondary structure, usually dominate exchange rates. Previous studies suggest that the NOS CaM-binding linker is unstructured and highly flexible in the absence of CaM [15, 16, 56, 57]. The large magnitude exchange suppression is consistent with CaM-binding inducing formation of the helix observed in reported co-structures of the CaM-bound iNOS linker [16]. The CaM-bound helix adjoins the FMN subdomain via a short hinge region containing the strictly conserved R752. Strong protection specific to the hinge is consistent with stabilization and reduced dynamics (Fig. 3b). CaM-binding also alters the structure and/or stability of regulatory interfaces. Most prominently, the CD2A hairpin undergoes striking deprotection. CD2A was proposed to influence the Ca^{2+}-dependency of nNOS activation via an ambiguous mechanism [20]. The CaM-induced effects on the CD2A hairpin suggest dissociation or deformation of the regulatory element.

A consistent finding of the HDX studies is that control of nNOS activation – via CaM-binding (Fig. 3) or phosphomimetics (Fig. 5) – impacts FMN subdomain structural dynamics. Multiple lines of evidence indicate that CaM binding promotes electronic deshielding of the FMN subdomain during NOS activation [45, 58]. Additionally, CaM binding is thought to promote release of the FMN subdomain from the rest of the reductase domain [7, 12, 14]. Here, we mapped specific FMN subdomain surfaces

deprotected by CaM binding, thereby supporting the hypothesis that CaM liberates the FMN subdomain from the FAD/NADPH binding lobe, shifting the conformational ensemble away from the input state.

NOS activation requires the enzyme to shuttle electrons productively between input and output state. Our data indicate a population shift away from the input state upon CaM-induced NOS activation, but evidence for a stabilized output state population is less evident. We observed CaM-induced exchange rate increases around the heme electron transfer access surface (Fig. 4). Increased exchange rates may be attributable to local conformational changes (e.g., rearrangements of backbone H-bonding) along the heme access surface during output state docking. Alternatively, this deprotection could reflect a global increase in nNOS structural dynamics upon CaM-induced catalytic cycling. Nevertheless, a stable oxygenase domain interface encompassing FMN subdomain and CaM docking sites was not apparent by HDX. Strikingly, this result contrasts with previous HDX-MS mappings of the iNOS output state inter-domain interactions [11]. However, the iNOS HDX-MS study employed domain truncations designed to promote formation of the output state. The more limited effects observed here for activated nNOS may be due to the transience of the output state interactions relative to the input state [12, 13, 45, 59]. Transient output state interactions relative to the input may be important for protecting reducing equivalents from NADPH from being transferred to alternative electron acceptors like dioxygen. Indeed, other enzymes with multi-domain diflavin reductase domain architectures, such as NADPH-cytochrome P450 oxidoreductase, exhibit similarly glancing interactions with redox partners [60, 61].

Previous fluorescence decay experiments suggest that nNOS exchanges between the input state and a neutral open state when inactive with only a small population of the output state sampled [13, 59]. Upon activation by CaM binding, the population shifts from the input state to the output state, but the open state still dominates. Furthermore, the lifetime of the output state is not enhanced upon activation, suggesting that a productive output state is transient [13]. In addition, productive orientation of the output state is thought to be governed by side-chain charges, an interaction that may not substantively influence the backbone amide protons measured by HDX [11, 44, 46]. Previous studies identified extensive oxygenase domain docking surfaces for productive

interdomain alignment, association, and electron transfer [7, 11, 46]. Nevertheless, the limited, localized output state "footprint" observed herein highlights the transience of the output state interface. A brief output state interaction would allow for rapid cycling of the FMN subdomain back to the input state for additional reducing equivalents to complete the synthesis of NO. Indeed, three distinct electron transfer events from FMN to heme are required for each NO molecule produced [62].

Transition between the input state and output state conformational regimes requires release of the FMN subdomain from the rest of the reductase domain. CaM binding and phosphomimetic mutations induced deuterium exchange increases, suggesting release of the FMN subdomain. Increased rates of electron transfer for phosphomimetic variants (with or without CaM) and CaM-bound nNOS WT also suggest a more dynamic FMN subdomain [9, 63, 64]. However, CaM is required for NO synthesis, suggesting the release of the FMN subdomain does not inherently coincide with a population shift toward the productive output state, but toward an open intermediate state. These findings agree with recent investigation by Dai, *et al*. exploring the critical roles of FMN subdomain dynamics and CaM-directed communication between nNOS domains [65]. Chemical crosslinking of the FMN subdomain to the FAD/NADPH subdomain dramatically attenuates the ability of CaM to stimulate electron transfer. Furthermore, lengthening the inter-domain linkers also diminishes CaM-induced activation.

Curiously, phosphomimetic variants of nNOS induce H/D exchange perturbations at the heme access point in the absence of CaM (Fig. 5, 6, Supplementary Fig. S6). This suggests that long-range allostery from the reductase domain primes the oxygenase domain for activity (or diminished activity in the case of S847D). In the context of FMN subdomain release and the transiency of the output state, our data suggest nNOS activation also requires a priming of the oxygenase conformation to prepare for interdomain electron transfer. For the S1412D variant, this allosteric priming manifests as an increase in exchange in the oxygenase domain, while the S847D variant exhibits an opposing decreased exchange. These changes in apparent oxygenase dynamics correlate with the increase of nNOS activity upon S1412 phosphorylation, and decrease for S847 phosphorylation [24, 51, 52, 66, 67]. Nevertheless, CaM binding is necessary and sufficient for eliciting the key conformational changes associated with

productive inter-domain electron trafficking (e.g., FMN subdomain release, productive oxygenase domain contact), relegating phosphorylation to role in tuning the degree of activation.

While the lifetime and occupancy of NOS conformational states has been explored using time-resolved fluorescence spectroscopy, questions remain regarding the influence of phosphorylation [13, 59]. We surmise that the decreased exchange rates manifest in the S847D variant (with and without CaM) indicate a shift toward a more stable output state. Indeed, removal of the AI, which contains S847, appears to stabilize the output state of CaM-bound nNOS [17, 22]. In the input state, the AI is positioned between the FMN- and NADPH-binding regions. Phosphorylation and CaM-binding may free the AI to stabilize the output state, hence the observed decrease in exchange rates as a function of S847D and CaM-binding. Conversely, S1412 phosphorylation may have the opposite effect of S847 phosphorylation. Rather than stabilizing the output state, S1412D may enhance the conformational flux of nNOS catalytic cycle. Accordingly, deletion of the CT, which includes S1412, promotes faster electron transport in the reductase domain, and small quantities of NO can be produced independent of CaM [21, 22]. This may indicate a more dynamic FMN subdomain without a stabilized output state. Future structural and spectroscopic interrogations of the role of the CT, AI, and phosphorylation may resolve these details.

Overall, our results reinforce the utility of HDX-MS as a tool for probing conformational changes and dynamics in large, multi-domain proteins. The NOS family proteins are prime examples of the challenges associated with deciphering the regulatory mechanisms of both signaling proteins and enzymes with elaborate electron transport systems. Hallmarks of both classes of proteins include multi-domain architectures with highly flexible linkers allowing for dynamic, regulated inter-domain communication. The large size and conformational heterogeneity of these enzymes present daunting obstacles to most structural biology approaches. HDX-MS is well-suited to probing dynamics in large, flexible proteins. Integrating HDX-MS data with the wealth of reported structures detailing individual enzyme domains provides a route to building higher-order models of complex enzyme activation mechanisms. Likewise, the integrative structural biology approach can illuminate cryptic allosteric pathways communicating regulatory protein interactions and post-translational modifications.

Materials and Methods

Protein Expression and Purification

All nNOS constructs were co-expressed with chaperone GroEL in BL21(DE3) cells in Terrific broth supplemented with 80 mM KH_2PO_2 pH 7.8. Cells were grown at 37 °C while shaking to $OD_{600\ nm}$ ~ 0.6. Cells were induced with 0.5 mM isopropyl β-D-1-thiogalactopyranoside (IPTG) supplemented with 0.45 mM ∂-aminolevulinic acid and 5 μM riboflavin to promote heme and FMN biosynthesis. Induced cells were incubated 35 hr at 20 °C while shaking. Cells were harvested by centrifugation and frozen at -80 °C. Frozen cell pellets were resuspended in 50 mM Tris pH 8.0, 5 mM DTT, 1 mM EDTA, 0.5 mM L-arginine, 10 μM H4B, 10% (v/v) glycerol then lysed using an Emulsiflex-C3 homogenizer. Insoluble cell debris was separated by centrifugation at 20,000 ×g for 60 min. Clarified lysates were supplemented with 2 mM $CaCl_2$ and applied to CaM-Sepharose 4B resin (GE Healthcare) preequilibrated with binding buffer (50 mM Tris pH 8.0, 5 mM DTT, 2 mM $CaCl_2$, 10 μM H4B, 10% (v/v) glycerol). The column was washed with binding buffer supplemented with 300 mM NaCl until the Abs_{280nm} baseline stabilized. Protein was eluted with 50 mM Tris pH 8.0, 250 mM NaCl, 5 mM DTT, 5 mM EGTA, 10 μM H4B, 10% (v/v) glycerol, concentrated in 10 kDa molecular weight cut-off (MWCO) spin concentrators, aliquoted, and snap frozen in liquid N_2. Protein concentration was determined using the Bradford assay with a BSA standard curve.

CaM was expressed in BL21(DE3) cells. Cells were grown at 37 °C with shaking to $OD_{600\ nm}$ ~ 0.6 and induced with 0.5 mM IPTG. Protein expression continued overnight at 28 °C with shaking. Cell harvesting and lysis was performed as with nNOS but with the substitution of a CaM lysis buffer (50 mM Tris pH 7.8, 100 mM NaCl, 2 mM $CaCl_2$, 1 mM DTT, 1 mM PMSF). Clarified cell lysate was applied to Phenyl Sepharose 6 FF resin (GE Healthcare) and further washed with CaM lysis buffer. CaM retained by the resin was further washed in a high salt buffer (50 mM Tris pH 7.8, 500 mM NaCl, 2 $CaCl_2$, 1 mM DTT). CaM was eluted in buffer supplemented with EGTA (50 mM Tris pH 7.8, 100 mM NaCl, 2 mM EGTA, 1 mM DTT). Elution fractions containing CaM, as assessed by SDS-PAGE, were pooled, concentrated in a 10 kDa MWCO spin concentrator, and buffer

exchanged into CaM storage buffer (50 mM HEPES pH 7.5, 100 mM NaCl, 1 mM DTT) using an Econo-Pac 10DG column (Bio-Rad). Buffer exchanged CaM was aliquoted, snap frozen in liquid N_2, and stored at -80 °C.

Hydrogen-Deuterium Exchange Mass Spectrometry

H/D exchange time courses were performed as previously described [39]. nNOS samples were buffer exchanged into 50 mM HEPES, pH 7.5, 100 mM NaCl, 1 mM DTT, 10 μM H4B and concentrated to 10 μM. H/D reactions done with CaM included 500 μM CaM before diluting into buffered D_2O. Deuterium exchange was initiated by dilution of protein stocks into buffered D_2O (50 mM HEPES, pD 7.5, 100 mM NaCl, 5 mM DTT). Exchange was quenched at 15, 45, 900, or 7200 s by addition of 5% (v/v) trifluoroacetic acid to pH 2.5 and flash freezing in liquid N_2. For digestion into uniquely identifiable peptides, each time point sample was rapidly thawed and digested using agarose-immobilized pepsin (Pierce) for 3 min at 4 °C in 0.025% TFA pH 2.5. Pepsin resin was removed by centrifugation, and samples were immediately refrozen in liquid N_2. Samples were stored at -80 °C until analysis. Pepsin digestion products were identified by LC-MS/MS as previously described [68]. Exchange samples were rapidly thawed immediately prior to injection into an Agilent 1260 HPLC equipped with a C8 reversed phase analytical column (Pinnacle DB 5 μm particle, 30 mm × 1 mm, Restek) connected in-line with a Q-Exactive Orbitrap (Thermo) mass spectrometer with a HESI-II electrospray ionization source (Thermo). Analytical column, inlet tubing, and injector were maintained at 0 °C - 4 °C and preequilibrated with 0.1% formic acid/10% ACN chilled to 4 °C. Peptides were eluted using a linear gradient from 10 – 25% over 2.5 min followed by 5.5 min ramp to 55% ACN. Mass spectra were collected in positive-mode (m/z range of 300-1,800) at a mass resolution setting of 70,000.

HDX-MS Data Analysis

HDX-MS data were processed and analyzed using HDX Workbench [69]. PyMol was used for imaging structures and mapping HDX-MS results. Exchange rate differences (Δ%D) are reported for a time point representative of the actively exchanging regime of

the timecourse. Statistical significance was determined using a two-tailed unpaired T-test [68].

Author Contributions

Q.M.H., J.R.C., and T.J.G conducted the experiments. Q.M.H. and E.S.U. designed the experiments and analyzed the data. Q.M.H., E.S.U., and B.C.S. wrote the paper.

Acknowledgements

We would like to thank Morgan C. Barrett for technical support. This work was partially supported by a National Science Foundation (CHE-1708829) grant to B.C.S.

References

[1] W. K. Alderton, Cooper C. E., Knowles R. G. (2001) Nitric oxide synthases: structure, function and inhibition. Biochem. J. 357, 593-615.

[2] E. D. Costa, Rezende B. A., Cortes S. F., Lemos V. S. (2016) Neuronal nitric oxide synthase in vascular physiology and diseases. Front. Physiol. 7.

[3] U. Förstermann, Sessa W. C. (2012) Nitric oxide synthases: regulation and function. Eur. Heart J. 33, 829-37.

[4] A. B. Knott, Bossy-Wetzel E. (2009) Nitric oxide in health and disease of the nervous system. Antioxid. Redox Signal. 11, 541-53.

[5] R. G. Keynes, Garthwaite J. (2004) Nitric oxide and its role in ischaemic brain injury. Curr. Mol. Med. 4, 179-91.

[6] A. V. Astashkin, Chen L., Zhou X., Li H., Poulos T. L., Liu K. J., et al. (2014) Pulsed electron paramagnetic resonance study of domain docking in neuronal nitric oxide synthase: the calmodulin and output state perspective. J. Phys. Chem. A. 118, 6864-72.

[7] M. G. Campbell, Smith B. C., Potter C. S., Carragher B., Marletta M. A. (2014) Molecular architecture of mammalian nitric oxide synthases. Proc. Natl. Acad. Sci. USA. 111, E3614-E23.

[8] C. Feng, Tollin G., Holliday M. A., Thomas C., Salerno J. C., Enemark J. H., et al. (2006) Intraprotein electron transfer in a two-domain construct of neuronal nitric oxide synthase: the output state in nitric oxide formation. Biochemistry. 45, 6354-62.

[9] R. P. Ilagan, Tiso M., Konas D. W., Hemann C., Durra D., Hille R., et al. (2008) Differences in a conformational equilibrium distinguish catalysis by the endothelial and neuronal nitric-oxide synthase flavoproteins. J. Biol. Chem. 283, 19603-15.

[10] E. Newman, Spratt D. E., Mosher J., Cheyne B., Montgomery H. J., Wilson D. L., et al. (2004) Differential activation of nitric-oxide synthase isozymes by calmodulin-troponin C chimeras. J. Biol. Chem. 279, 33547-57.

[11] B. C. Smith, Underbakke E. S., Kulp D. W., Schief W. R., Marletta M. A. (2013) Nitric oxide synthase domain interfaces regulate electron transfer and calmodulin activation. Proc. Natl. Acad. Sci. USA. 110, E3577-86.

[12] Y. He, Haque M. M., Stuehr D. J., Lu H. P. (2015) Single-molecule spectroscopy reveals how calmodulin activates NO synthase by controlling its conformational fluctuation dynamics. Proc. Natl. Acad. Sci. USA. 112, 11835-40.

[13] J. C. Salerno, Ray K., Poulos T., Li H., Ghosh D. K. (2013) Calmodulin activates neuronal nitric oxide synthase by enabling transitions between conformational states. FEBS Lett. 587, 44-7.

[14] A. L. Yokom, Morishima Y., Lau M., Su M., Glukhova A., Osawa Y., et al. (2014) Architecture of the nitric-oxide synthase holoenzyme reveals large conformational changes and a calmodulin-driven release of the FMN domain. J. Biol. Chem. 289, 16855-65.

[15] M. Piazza, Dieckmann T., Guillemette J. G. (2016) Structural Studies of a Complex Between Endothelial Nitric Oxide Synthase and Calmodulin at Physiological Calcium Concentration. Biochemistry. 55, 5962-71.

[16] C. Xia, Misra I., Iyanagi T., Kim J. J. (2009) Regulation of interdomain interactions by calmodulin in inducible nitric-oxide synthase. The Journal of biological chemistry. 284, 30708-17.

[17] C. Feng, Roman L. J., Hazzard J. T., Ghosh D. K., Tollin G., Masters B. S. S. (2008) Deletion of the autoregulatory insert modulates intraprotein electron transfer in rat neuronal nitric oxide synthase. FEBS Lett. 582, 2768-72.

[18] H. J. Montgomery, Romanov V., Guillemette J. G. (2000) Removal of a putative inhibitory element reduces the calcium-dependent calmodulin activation of neuronal nitric-oxide synthase. J. Biol. Chem. 275, 5052-8.

[19] J. C. Salerno, Harris D. E., Irizarry K., Patel B., Morales A. J., Smith S. M., et al. (1997) An autoinhibitory control element defines calcium-regulated isoforms of nitric oxide synthase. J. Biol. Chem. 272, 29769-77.

[20] G. M. Knudsen, Nishida C. R., Mooney S. D., de Montellano P. R. O. (2003) Nitric-oxide synthase (NOS) reductase domain models suggest a new control element in

endothelial NOS that attenuates calmodulin-dependent activity. J. Biol. Chem. 278, 31814-24.

[21] M. Tiso, Tejero J., Panda K., Aulak K. S., Stuehr D. J. (2007) Versatile regulation of neuronal nitric oxide synthase by specific regions of its C-terminal tail. Biochemistry. 46, 14418-28.

[22] L. J. Roman, Masters B. S. (2006) Electron transfer by neuronal nitric-oxide synthase is regulated by concerted interaction of calmodulin and two intrinsic regulatory elements. J. Biol. Chem. 281, 23111-8.

[23] E. D. Garcin, Bruns C. M., Lloyd S. J., Hosfield D. J., Tiso M., Gachhui R., et al. (2004) Structural basis for isozyme-specific regulation of electron transfer in nitric-oxide synthase. J. Biol. Chem. 279, 37918-27.

[24] K. Komeima, Hayashi Y., Naito Y., Watanabe Y. (2000) Inhibition of neuronal nitric-oxide synthase by calcium/ calmodulin-dependent protein kinase IIalpha through Ser847 phosphorylation in NG108-15 neuronal cells. J. Biol. Chem. 275, 28139-43.

[25] J. Igarashi, Li H., Jamal J., Ji H., Fang J., Lawton G. R., et al. (2009) Crystal structures of constitutive nitric oxide synthases in complex with de novo designed inhibitors. J. Med. Chem. 52, 2060-6.

[26] H. Li, Jamal J., Plaza C., Pineda S. H., Chreifi G., Jing Q., et al. (2014) Structures of human constitutive nitric oxide synthases. Acta Crystallogr. Sect. D. Biol. Crystallogr. 70, 2667-74.

[27] C. Raman, Li H., Martásek P., Southan G., Masters B. S. S., Poulos T. L. (2001) Crystal structure of nitric oxide synthase bound to nitro indazole reveals a novel inactivation mechanism. Biochemistry. 40, 13448-55.

[28] R. J. Rosenfeld, Garcin E. D., Panda K., Andersson G., Åberg A., Wallace A. V., et al. (2002) Conformational changes in nitric oxide synthases induced by chlorzoxazone and nitroindazoles: crystallographic and computational analyses of inhibitor potency. Biochemistry. 41, 13915-25.

[29] J. R. Engen. Analysis of protein conformation and dynamics by hydrogen/deuterium exchange MS. ACS Publications; 2009.

[30] C. M. Hebling, Morgan C. R., Stafford D. W., Jorgenson J. W., Rand K. D., Engen J. R. (2010) Conformational analysis of membrane proteins in phospholipid bilayer nanodiscs by hydrogen exchange mass spectrometry. Anal. Chem. 82, 5415-9.

[31] R. E. Joseph, Wales T. E., Fulton D. B., Engen J. R., Andreotti A. H. (2017) Achieving a Graded Immune Response: BTK Adopts a Range of Active/Inactive Conformations Dictated by Multiple Interdomain Contacts. Structure. 25, 1481-94. e4.

[32] L. Konermann, Pan J., Liu Y. H. (2011) Hydrogen exchange mass spectrometry for studying protein structure and dynamics. Chem Soc Rev. 40, 1224-34.

[33] D. P. Marciano, Dharmarajan V., Griffin P. R. (2014) HDX-MS guided drug discovery: small molecules and biopharmaceuticals. Curr. Opin. Struct. Biol. 28, 105-11.

[34] A. J. Percy, Rey M., Burns K. M., Schriemer D. C. (2012) Probing protein interactions with hydrogen/deuterium exchange and mass spectrometry—a review. Anal. Chim. Acta. 721, 7-21.

[35] M. L. Eisinger, Dörrbaum A. R., Michel H., Padan E., Langer J. D. (2017) Ligand-induced conformational dynamics of the Escherichia coli Na+/H+ antiporter NhaA revealed by hydrogen/deuterium exchange mass spectrometry. Proc. Natl. Acad. Sci. USA. 201703422.

[36] R. E. Iacob, Pene-Dumitrescu T., Zhang J., Gray N. S., Smithgall T. E., Engen J. R. (2009) Conformational disturbance in Abl kinase upon mutation and deregulation. Proc. Natl. Acad. Sci. USA. 106, 1386-91.

[37] J. G. Sheff, Farshidfar F., Bathe O. F., Kopciuk K., Gentile F., Tuszynski J., et al. (2017) Novel Allosteric Pathway of Eg5 Regulation Identified through Multivariate Statistical Analysis of Hydrogen-Exchange Mass Spectrometry (HX-MS) Ligand Screening Data. Molecular & Cellular Proteomics. 16, 428-37.

[38] Y. Xiao, Shaw G. S., Konermann L. (2017) Calcium-Mediated Control of S100 Proteins: Allosteric Communication via an Agitator/Signal Blocking Mechanism. J. Am. Chem. Soc.

[39] E. S. Underbakke, Iavarone A. T., Chalmers M. J., Pascal B. D., Novick S., Griffin P. R., et al. (2014) Nitric oxide-induced conformational changes in soluble guanylate cyclase. Structure. 22, 602-11.

[40] J. Garthwaite. (2008) Concepts of neural nitric oxide- mediated transmission. Eur. J. Neurosci. 27, 2783-802.

[41] N. Hardingham, Dachtler J., Fox K. (2013) The role of nitric oxide in pre-synaptic plasticity and homeostasis. Front Cell Neurosci. 7, 1-19.

[42] K. Chachlaki, Garthwaite J., Prevot V. (2017) The gentle art of saying NO: how nitric oxide gets things done in the hypothalamus. Nat Rev Endocrinol. 13, 521-35.

[43] P. Mukherjee, Cinelli M. A., Kang S., Silverman R. B. (2014) Development of nitric oxide synthase inhibitors for neurodegeneration and neuropathic pain. Chem. Soc. Rev. 43, 6814-38.

[44] S. A. Hollingsworth, Holden J. K., Li H., Poulos T. L. (2016) Elucidating nitric oxide synthase domain interactions by molecular dynamics. Protein Sci. 25, 374-82.

[45] J. Tejero, Haque M. M., Durra D., Stuehr D. J. (2010) A bridging interaction allows calmodulin to activate NO synthase through a bi-modal mechanism. J. Biol. Chem. 285, 25941-9.

[46] J. Tejero, Hannibal L., Mustovich A., Stuehr D. J. (2010) Surface charges and regulation of FMN to heme electron transfer in nitric-oxide synthase. J. Biol. Chem. 285, 27232-40.

[47] G. A. Rameau, Chiu L.-Y., Ziff E. B. (2004) Bidirectional regulation of neuronal nitric-oxide synthase phosphorylation at serine 847 by the N-methyl-D-aspartate receptor. J. Biol. Chem. 279, 14307-14.

[48] S. Gingerich, Krukoff T. L. (2008) Activation of ERβ increases levels of phosphorylated nNOS and NO production through a Src/PI3K/Akt-dependent pathway in hypothalamic neurons. Neuropharmacology. 55, 878-85.

[49] K. J. Hurt, Sezen S. F., Lagoda G. F., Musicki B., Rameau G. A., Snyder S. H., et al. (2012) Cyclic AMP-dependent phosphorylation of neuronal nitric oxide synthase mediates penile erection. Proc. Natl. Acad. Sci. USA. 109, 16624-9.

[50] L. Sánchez-Ruiloba, Aicart-Ramos C., García-Guerra L., Pose-Utrilla J., Rodríguez-Crespo I., Iglesias T. (2014) Protein kinase D interacts with neuronal nitric oxide synthase and phosphorylates the activatory residue serine1412. PloS one. 9, e95191.

[51] G. A. Rameau, Tukey D. S., Garcin-Hosfield E. D., Titcombe R. F., Misra C., Khatri L., et al. (2007) Biphasic coupling of neuronal nitric oxide synthase phosphorylation to the NMDA receptor regulates AMPA receptor trafficking and neuronal cell death. J. Neurosci. 27, 3445-55.

[52] Y. Hayashi, Nishio M., Naito Y., Yokokura H., Nimura Y., Hidaka H., et al. (1999) Regulation of neuronal nitric-oxide synthase by calmodulin kinases. J. Biol. Chem. 274, 20597-602.

[53] S. Adak, Santolini J., Tikunova S., Wang Q., Johnson J. D., Stuehr D. J. (2001) Neuronal nitric-oxide synthase mutant (Ser-1412→ Asp) demonstrates surprising connections between heme reduction, NO complex formation, and catalysis. J. Biol. Chem. 276, 1244-52.

[54] T. Vorherr, Knoepfel L., Hofmann F., Mollner S., Pfeuffer T., Carafoli E. (1993) The calmodulin binding domain of nitric oxide synthase and adenylyl cyclase. Biochemistry. 32, 6081-8.

[55] G. Wu, Berka V., Tsai A.-L. (2011) Binding kinetics of calmodulin with target peptides of three nitric oxide synthase isozymes. J. Inorg. Biochem. 105, 1226-37.

[56] M. Piazza, Taiakina V., Guillemette S. R., Guillemette J. G., Dieckmann T. (2014) Solution structure of calmodulin bound to the target peptide of endothelial nitric oxide synthase phosphorylated at Thr495. Biochemistry. 53, 1241-9.

[57] M. Zhang, Vogel H. J. (1994) Characterization of the calmodulin-binding domain of rat cerebellar nitric oxide synthase. J. Biol. Chem. 269, 981-5.

[58] R. P. Ilagan, Tejero J., Aulak K. S., Ray S. S., Hemann C., Wang Z. Q., et al. (2009) Regulation of FMN subdomain interactions and function in neuronal nitric oxide synthase. Biochemistry. 48, 3864-76.

[59] D. K. Ghosh, Ray K., Rogers A. J., Nahm N. J., Salerno J. C. (2012) FMN fluorescence in inducible NOS constructs reveals a series of conformational states involved in the reductase catalytic cycle. FEBS J. 279, 1306-17.

[60] D. Hamdane, Xia C., Im S.-C., Zhang H., Kim J.-J. P., Waskell L. (2009) Structure and function of an NADPH-cytochrome P450 oxidoreductase in an open conformation capable of reducing cytochrome P450. J. Biol. Chem. 284, 11374-84.

[61] M. Sugishima, Sato H., Higashimoto Y., Harada J., Wada K., Fukuyama K., et al. (2014) Structural basis for the electron transfer from an open form of NADPH-cytochrome P450 oxidoreductase to heme oxygenase. Proc. Natl. Acad. Sci. USA. 111, 2524-9.

[62] E. S. Underbakke, Sürmeli N. B., Smith B. C., Wynia-Smith S. L., Marletta M. A. Nitric Oxide Signaling. In: Reedijk J, Poeppelmeier K, editors. Comprehensive Inorganic Chemistry II. Oxford: Elsevier; 2013. p. 241-62.

[63] A. J. Dunford, Rigby S. E., Hay S., Munro A. W., Scrutton N. S. (2007) Conformational and thermodynamic control of electron transfer in neuronal nitric oxide synthase. Biochemistry. 46, 5018-29.

[64] C. Feng, Chen L., Li W., Elmore B. O., Fan W., Sun X. (2014) Dissecting regulation mechanism of the FMN to heme interdomain electron transfer in nitric oxide synthases. J. Inorg. Biochem. 130, 130-40.

[65] Y. Dai, Haque M. M., Stuehr D. J. (2017) Restricting the conformational freedom of the neuronal nitric-oxide synthase flavoprotein domain reveals impact on electron transfer and catalysis. J. Biol. Chem. 292, 6753-64.

[66] P. F. Mount, Fraser S. A., Watanabe Y., Lane N., Katsis F., Chen Z.-P., et al. (2006) Phosphorylation of neuronal and endothelial nitric oxide synthase in the kidney with high and low salt diets. Nephron Physiol. 102, p36-p50.

[67] K. Osuka, Watanabe Y., Usuda N., Atsuzawa K., Takayasu M. (2013) Phosphorylation of neuronal nitric oxide synthase at Ser 1412 in the dentate gyrus of rat brain after transient forebrain ischemia. Neurochem. Int. 63, 269-74.

[68] E. S. Underbakke, Iavarone A. T., Marletta M. A. (2013) Higher-order interactions bridge the nitric oxide receptor and catalytic domains of soluble guanylate cyclase. Proc. Natl. Acad. Sci. USA. 110, 6777-82.

[69] B. D. Pascal, Willis S., Lauer J. L., Landgraf R. R., West G. M., Marciano D., et al. (2012) HDX Workbench: software for the analysis of H/D exchange MS data. J. Am. Soc. Mass Spectrom. 23, 1512-21.

Figure Legends

Fig. 1. NOS domain organization and conformational states. (a) NOS isoforms are composed of an N-terminal oxygenase domain, a C-terminal reductase domain, and an intervening CaM-binding linker. The oxygenase mediates homodimerization and encloses the active site heme. The reductase domain is further divided into an FAD/NADPH subdomain and a mobile FMN subdomain. The nNOS isoform also includes an N-terminal PDZ domain (not pictured) for synaptic localization. (b) CaM-binding promotes the productive shuttling of the FMN subdomain between input and output states to deliver electrons from the reductase domain to the oxygenase domain. In the input state the FMN subdomain associates with the NADPH/FAD subdomain, allowing transfer of reducing equivalents from NADPH to FAD to FMN. In the output state FMN transiently associates with the oxygenase domain of the other homodimer subunit, to allow electron transfer from FMN to heme.

Fig. 2. CaM-induced exchange rate perturbations in nNOS. Peptide coverage is represented by bars mapped to primary sequence with every twentieth residue noted in white. Exchange rate perturbations are reported as the average difference in %D incorporation at time points approximating the midpoint of exchange. Peptides exhibiting significant (p<0.05) exchange rate perturbations are color coded according to the scale bar (top). Significance was assessed with a two-tailed unpaired Student's t test. Peptides exhibiting undetectable or nonsignificant differences in exchange are colored in grey. Sites of phosphorylation are noted in red. Residues W587 and R752 are highlighted in yellow and purple, respectively.

Fig. 3. CaM-Induced conformational changes mapped onto the nNOS reductase domain. Calmodulin induces conformational changes in nNOS reductase domain. All images are color coded to according to the scale bar to indicate change in %D. (a) HDX results mapped on to the human iNOS CaM-FMN subdomain structure (PDB 3HR4). Key features are emphasized by highlighting. Yellow spheres represent CaM-bound Ca^{2+}. (b) R752 coordinates a hydrogen bonding network between CaM and the FMN

subdomain. NOS residues are numbered according to rat nNOS, not iNOS. For clarity, nitrogen atoms in panel B are colored yellow rather than the standard blue (c) HDX results mapped to the structure of the nNOS reductase domain (PDB 1TLL). Perturbations localize primarily to the FMN subdomain, outlined in light green. (d) A hydrophobic pocket around the AI undergoes CaM-induced perturbations. (e) The obverse surface of the nNOS reductase domain, where the CT is localized, is perturbed in a CaM-induced manner.

Fig. 4. CaM-induced conformational changes mapped to the nNOS oxygenase domain (a) CaM-induced perturbations in WT nNOS mapped on to the oxygenase domain structure (PBD: 1OM4). Arrow points to heme electron transfer access point. Perturbations were color coded according to the scale bar below. The oxygenase domain dimer interface is marked with a dotted line. (b) Close-up of the heme access point. Residues 416-424 form the lower “lip” of the heme access point. W587 (side chain shown, nitrogen colored blue) is a key residue that coordinates electron transfer from FMN to the heme. Heme is represented as red stick models.

Fig. 5. Phosphomimetic-induced conformational perturbations mapped to nNOS domain models. H/D exchange rates of CaM-activated nNOS S847D or S1412D were compared to CaM-activated nNOS WT were measured and mapped to NOS domain models. Exchange rate differences (Δ%D) were color coded according to the scale bar. Left column: Increased protection of the CaM-binding helix due to phosphomimetic mutations are mapped to the corresponding residues of the human iNOS CaM-FMN subdomain co-structure (PDB: 3HR4). Middle: Reductase domain perturbations are localized to FMN subdomain (outlined in light green) for both phosphomimetic variants. Exchange rate differences were mapped to the nNOS reductase domain (PDB: 1TLL) with the iNOS CaM-binding region (PDB: 3HR4) modelled in using PyMol. Cofactors are shown as yellow stick models. Right column: Exchange rate perturbations mapped on to nNOS oxygenase domain (PDB: 1OM4) reveal differing oxygenase domain dynamics for nNOS S847D and S1412D. Heme is represented by red stick models.

Fig. 6. Localizing activation-associated conformational perturbations to nNOS domains. Exchange rate perturbations associated with CaM-binding or phosphomimetics were condensed and mapped to a cartoon representation of the nNOS domain organization. Differences in %D incorporation are color-coded according to the scale bar below.

Highlights

- Mechanisms of nitric oxide synthase (NOS) activation and regulation are ambiguous
- Ca^{2+}/calmodulin (CaM) and phosphorylation regulate nNOS function
- H/D exchange MS dissects structural mechanism of nNOS activation and regulation
- CaM induces FMN subdomain conformational changes via linker ordering
- CaM allows allosteric communication between reductase and oxygenase domains
- Phosphomimetics prime nNOS for activity independent of calmodulin

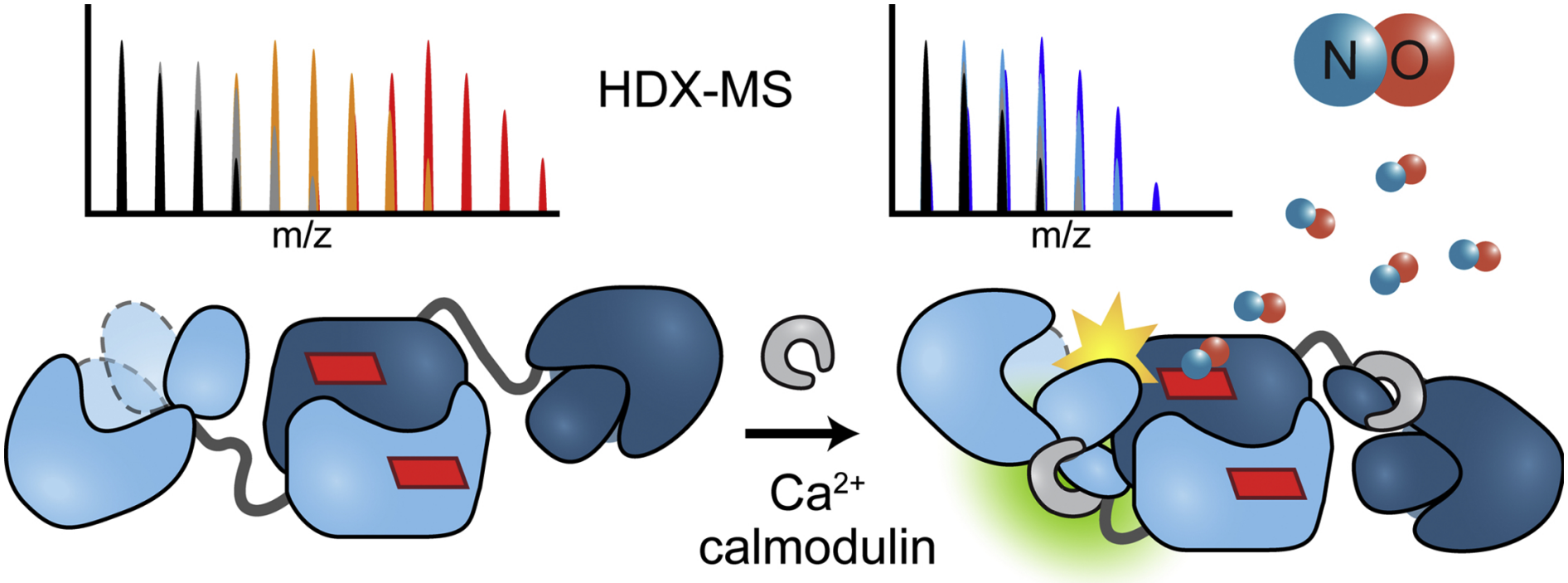

Graphics Abstract

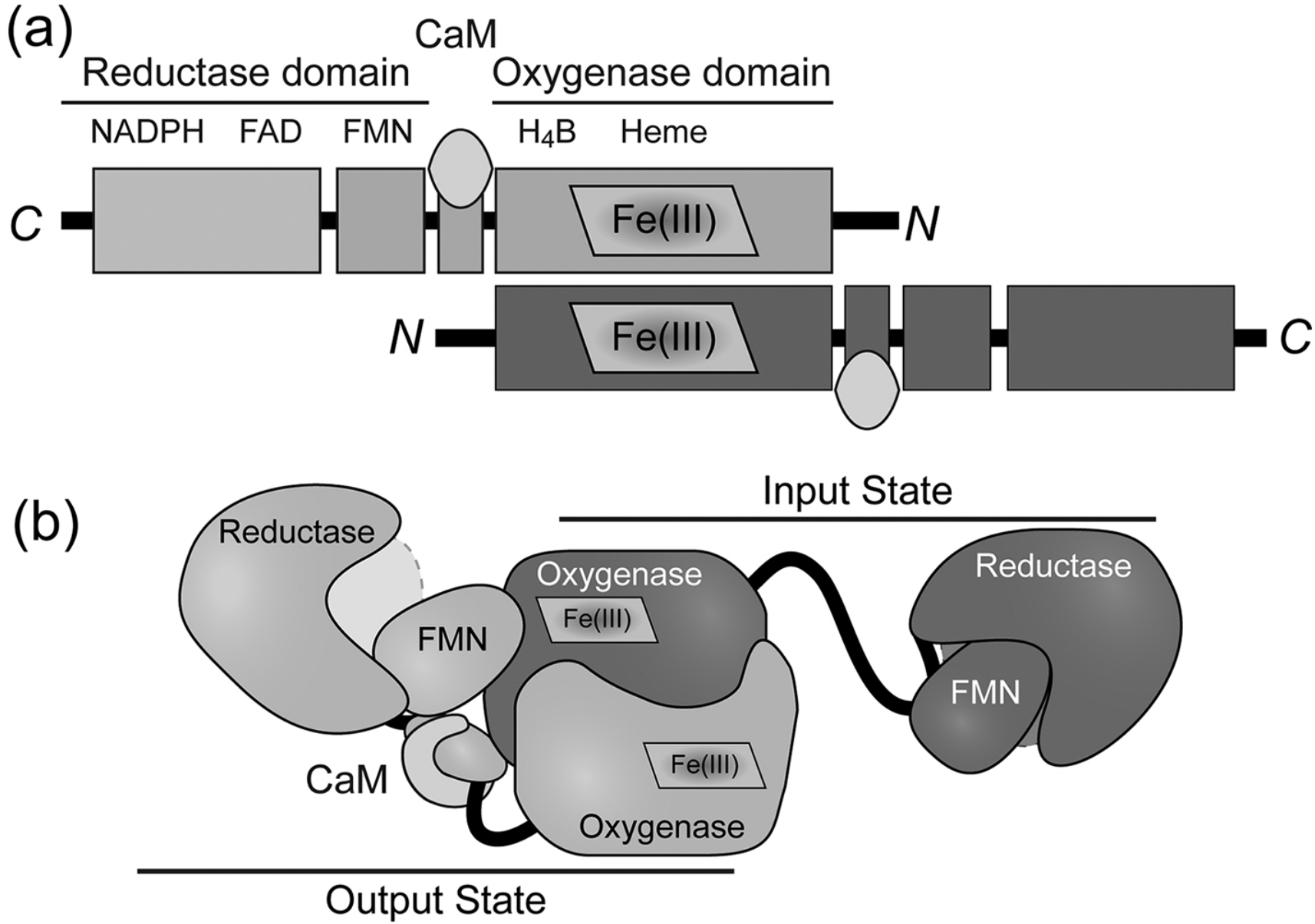
(a)
CaM
Reductase domain
Oxygenase domain
NADPH
FAD
FMN
H4B
Heme
C
Fe(III)
N
N
Fe(III)
C
(b)
Input State
Reductase
Oxygenase
Fe(III)
FMN
Reductase
FMN
CaM
Fe(III)
Oxygenase
Output State

Figure 1

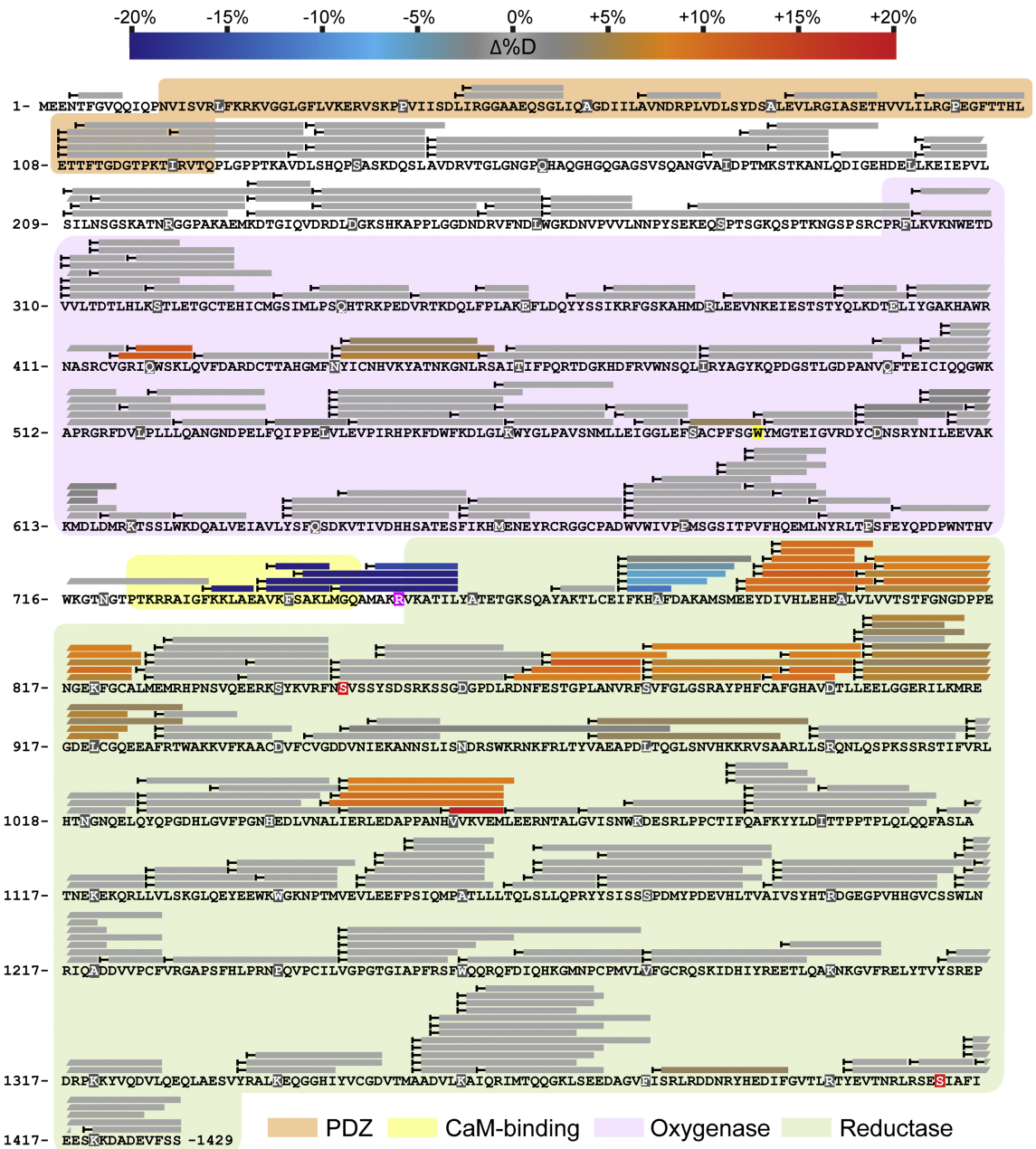
-20%
-15%
-10%
-5%
0%
+5%
+10%
+15%
+20%
Δ%D
1- MEENTFGVQQIQPNVISVRLFKRKVGGLGFLVKERVSKPPVIISDLIRGGAAEQSGLIQAGDIILAVNDRPLVDLSYDSALEVLRGIASETHVVLILRGPEGFTTHL
108- ETTFTGDGTPKTIRVTQPLGPPTKAVDLSHQPSASKDQSLAVDRVTGLGNGPQHAQGHGQGAGSVSQANGVAIDPTMKSTKANLQDIGEHDELLKEIEPVL
209- SILNSGGSKATNRGGPAKAEMKDTGIQVDRDLDGKSHKAPPLGGDNDRVFNDLWGKDNVPVVLNNPYSEKEQSPTSGKQSPTKNGSPSRCPRGLKVKNWETD
310- VVLTDTLHLKSTLETGCTEHICMGSIMLPSQHTRKPEDVRTKDQLFPLAKEFLDQYYSSIKRFGSKAHMDRLEEVNKEIESTSTYQLKDTELIYGAKHAWR
411- NASRCVGRIQWSKLQVFDARDCTTAHGMFNYICNHVKYATNKGNLRSAITIFPQRTDGKHDFRVWNSQLIRYAGYKQPDGSTLGDPANVQFTEICIQQGWK
512- APRGRFDVLPLLLQANGNDPELFQIPPELVLEVPIRHPKFDWFKDLGLKWYGLPAVSNMLLEIGGLEFSACPFSGWYMGTEIGVRDYCDNSRYNILEEVAK
613- KMDLDMRKTSSLWKDQALVEIAVLYSFQSDKVTIVDHHSATESFIKHVMENEYRCRGGCPADWVWIVPPMSGSITPVFHQEMLNYRLTPSFEYQPDPWNTHV
716- WKGTNGTPTKRRAIGFKKLAEAVKFSAKLMGQAMAKRVKATILYATETGKSQAYAKTLCEIFKHAFDAKAMSMEEYDIVHLEHEALVLVVTSTFGNGDPPE
817- NGEKFGCALMEMRHPNSVQEERKSYKVRFNSVSSYSDSRKSSGDGPDLRDNFESTGPLANVRFSVFGLGSRAYPHFCAFGHAVDTLLEELGGERILKMRE
917- GDELCGQEEAFRTWAKKVFKAACDVFCVGDDVNIEKANNSLISNDRSWKRNKFRLTYVAEAPDLTQGLSNVHKKRVSAARLLSRQNLQSPKSSRSTIFVRL
1018- HTNGNQELQYQPGDHLGVFPGNHEDLVNALIERLEDAPPANHVVKVEMLEERNTALGVISNWKDESRLPPCTIFQAFKYYLDITTPPTPLQLQQFASLA
1117- TNEKEKQRLLVLSKGLQEYEEWKWGKNPTMVEVLEEFPSIQMPATLLLTQLSLLQPRYYSISSSPDMYPDEVHLTVAIVSYHTRDGEGPVHHGVCSSWLN
1217- RIQADDVVPCFVRGAPSFHLPRNPQVPCILVGPGTGIAPFRSFWQQRQFDIQHKGMNPCPMVLVFGCRQSKIDHIYREETLQAKNKGVFRELYTVYSREP
1317- DRPKKYVQDVLQEQLAESVYRALKEQGGHIYVCGDVTMAADVLKAIQRIMTQQGKLSEEDAGVEISRLRDDNRYHEDIFGVTLRTYEVTNRLRSESIAFI
1417- EESKKDADEVFSS -1429
PDZ
CaM-binding
Oxygenase
Reductase

Figure 2

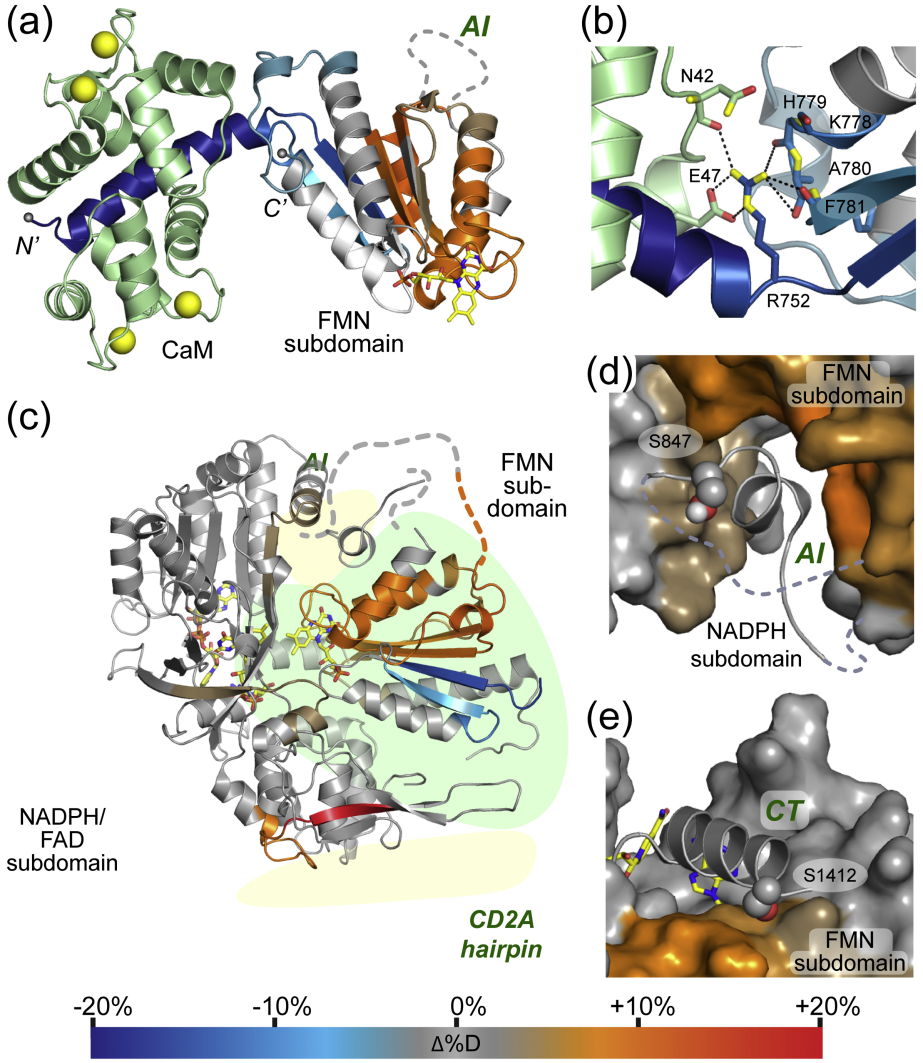
(a)
AI
C'
N'
CaM
FMN
subdomain
(b)
N42
H779
K778
E47
A780
F781
R752
(c)
AI
FMN
sub-
domain
NADPH/
FAD
subdomain
CD2A
hairpin
(d)
FMN
subdomain
S847
AI
NADPH
subdomain
(e)
CT
S1412
FMN
subdomain
-20%
-10%
0%
+10%
+20%
Δ%D

Figure 3

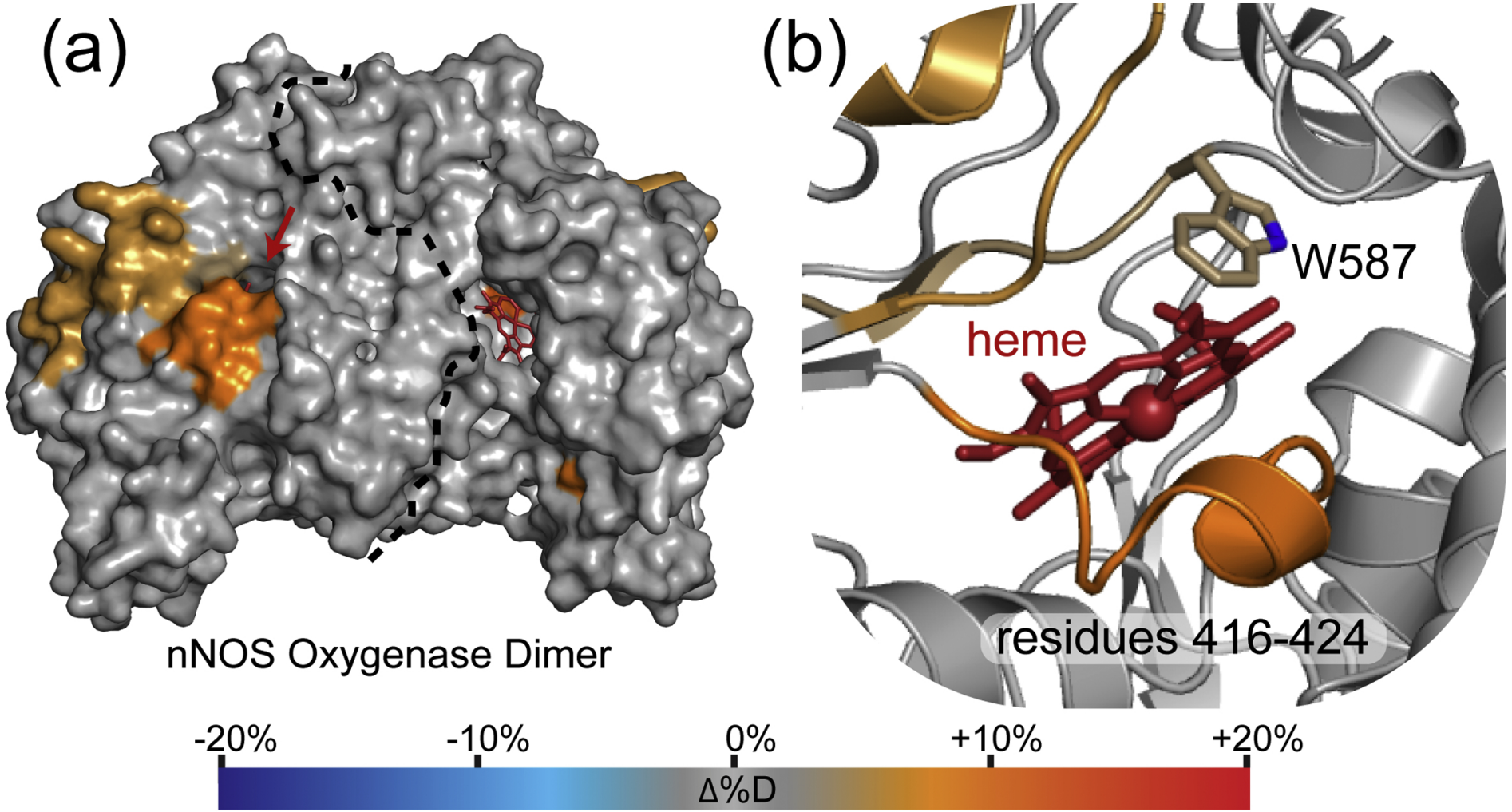
(a)
nNOS Oxygenase Dimer
(b)
W587
heme
residues 416-424
-20%
-10%
0%
+10%
+20%
Δ%D

Figure 4

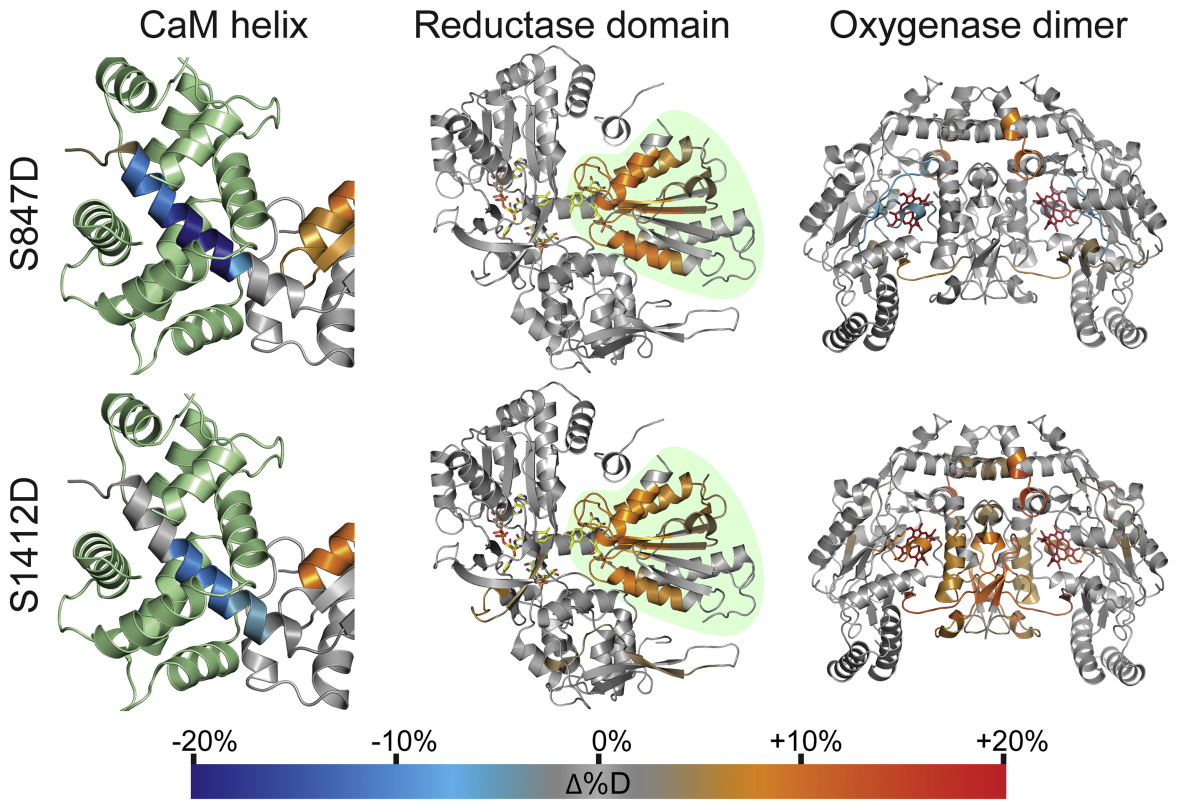
CaM helix
Reductase domain
Oxygenase dimer
S847D
S1412D
-20%
-10%
0%
+10%
+20%
Δ%D

Figure 5

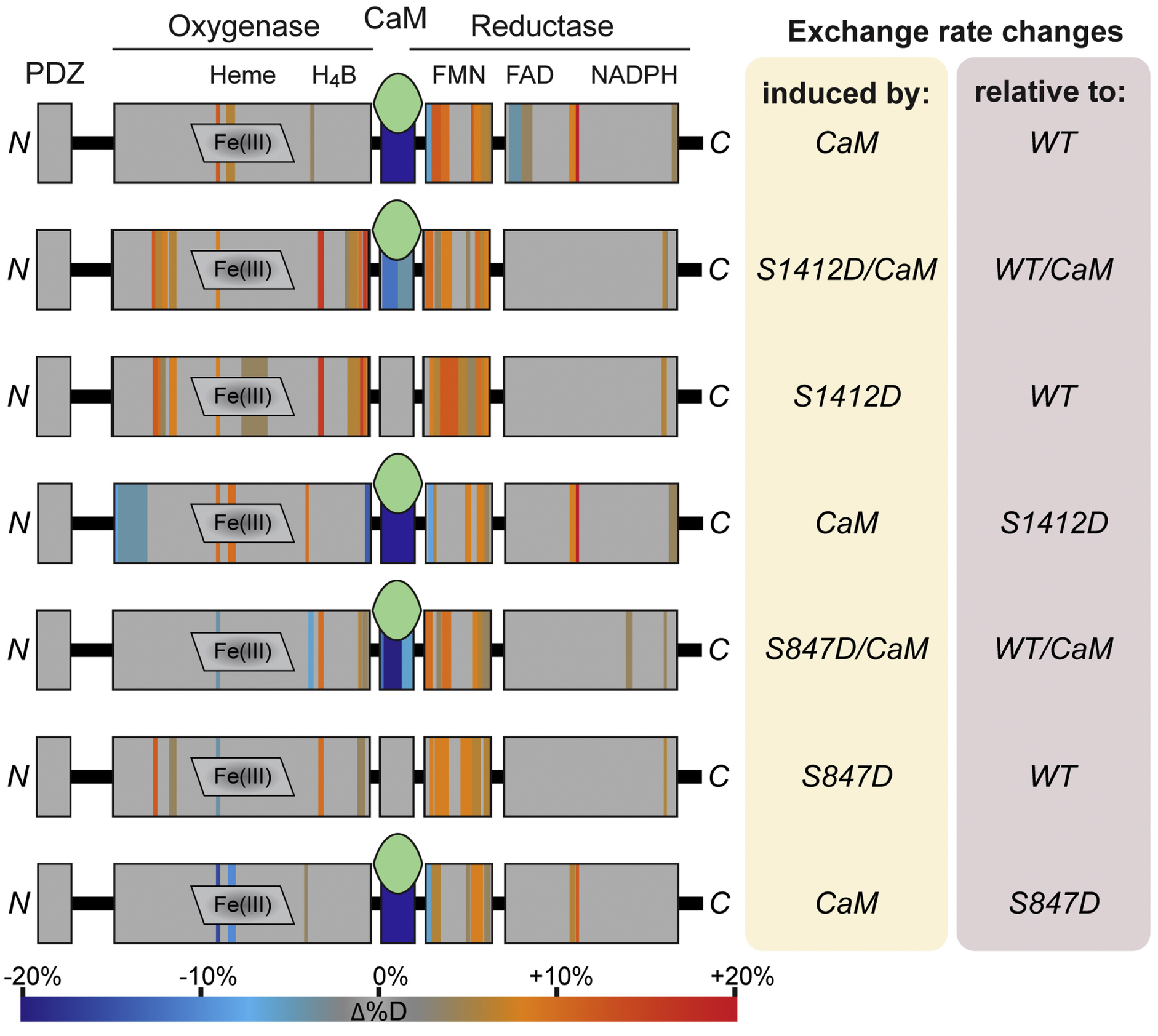
Oxygenase
CaM
Reductase
PDZ
Heme
H4B
FMN
FAD
NADPH
N
C
Fe(III)
Exchange rate changes
induced by:
relative to:
CaM
WT
S1412D/CaM
WT/CaM
S1412D
WT
CaM
S1412D
S847D/CaM
WT/CaM
S847D
WT
CaM
S847D
-20%
-10%
0%
+10%
+20%
Δ%D

Figure 6